Talanta 85 (2011) 2202–2211

Contents lists available at ScienceDirect

Talanta

journal homepage: www.elsevier.com/locate/talanta

The effects of carbon nanotubes on the electrocatalysis of hydrogen peroxide by metallo-phthalocyanines

Philani Mashazi[a,b], Tawanda Mugadza[b], Ndabenhle Sosibo[a], Phumlani Mdluli[a], Sibulelo Vilakazi[a], Tebello Nyokong[b,*]

[a] Nanotechnology Innovation Centre, Advanced Materials Division, Mintek, Private Bag X3015, Randburg 2125, South Africa
[b] Nanotechnology Innovation Centre – Sensors, Chemistry Department, Rhodes University, PO Box 94, Grahamstown 6140, South Africa

ARTICLE INFO

Article history:
Received 31 May 2011
Received in revised form 19 July 2011
Accepted 20 July 2011
Available online 27 July 2011

Keywords:
Single-wall carbon nanotubes
Metal tetra-amino phthalocyanine
Electroanalysis
Hydrogen peroxide

ABSTRACT

The pre-grafted screen-printed gold electrode modified with phenyl-amino monolayer was investigated for covalent immobilization of phenyl-amine functionalized single-walled carbon nanotubes (PA-SWCNT) and metal tetra-amino phthalocyanine (MTAPc) using Schiff-base reactions with benzene-1,4-dicarbaldehyde (BDCA) as cross-linker. The PA-SWCNT and MTAPc modified electrodes were applied as hybrids for electrochemical sensing of H_2O_2. The step-by-step fabrication of the electrode was followed using electrochemistry, impedance spectroscopy, scanning electron microscopy and Raman spectroscopy and all these techniques confirmed the fabrication and the immobilization of PA-SWCNT, MnTAPc and CoTAPc onto gold surfaces. The apparent electron transfer constant (k_{app}) showed that the carbon nanotubes and metallo-phthalocyanines hybrids possess good electron transfer properties compared to the bare, pre-grafted and the MTAPc modified gold electrode surfaces without PA-SWCNT. The electrochemical sensing of hydrogen peroxide was successful with PA-SWCNT–MTAPc hybrid systems showing higher electrocatalytic currents compared to the other electrodes. The analytical parameters obtained using chronoamperometry gave good linearity at H_2O_2 concentrations ranging from 1.0 to 30.0 μmol L^{-1}. The values for the limit of detection (LoD) were found to be of the orders of 10^{-7} M using the 3δ for all the electrodes. The PA-SWCNT–MTAPc modified SPAuEs were much more sensitive compared to PA–MTAPc modified SPAuEs.

1. Introduction

Hydrogen peroxide (H_2O_2) is a strong chemical oxidant. In clinical and biomedical applications, H_2O_2 is a by-product of many enzymatic reactions [1], for example during the conversion of glucose to gluconolactone [2]. Therefore, the detection and monitoring of the levels of H_2O_2 is of importance and amongst various methods that are used, electrochemical methods are favoured. The preference of electrochemical method is due to their simplicity and potential of miniaturizing the final devices for the ease of portability. This work investigates the use of nano-structured materials (carbon nanotubes) in conjunction with synthetic compounds (metallo-phthalocyanines) as hybrids for electrochemical detection and monitoring of H_2O_2.

The fabrication of screen-printed gold electrodes with metal tetra-amino phthalocyanine (MTAPc) complexes containing cobalt (CoTAPc) and manganese (MnTAPc) as metal ion centres was investigated recently for the detection of H_2O_2 [3]. In our previous studies, we have demonstrated the immobilization of the MTAPc complexes onto electrode surfaces using electropolymerization [4] and monolayer covalent attachment onto phenyl-amine pre-grafted electrode surface [3]. The latter method was preferred to electropolymerization as it gave control of surface modification and it yielded very stable monolayer thin films. Carbon nanotubes are highly conjugated systems with good material strength [5]. The application of carbon nanotubes in electrochemistry is due to their good conducting and electron-transfer properties with good chemical and thermal resistance. The majority of electrochemical studies on single walled carbon nanotubes involve their immobilization using drop-dry or drop-coating method onto carbon electrode surfaces [6,7] and covalent attachment onto thiol self-assembled monolayer functionalized gold surfaces [8]. The self-assembly monolayer (SAM) method gives good control of the surface functionalization, especially gold surfaces; however SAMs lack stability and are mobile on the electrode surfaces. Electrografting, as an alternative stable method of modifying electrode surfaces, uses functionalized aryl diazonium salt to form molecular thick monolayer [3]. Electrografting has similar advantages as SAMs as it gives control of the surface functionalization but the formed monolayers are more stable.

* Corresponding author. Tel.: +27 46 603 8260; fax: +27 46 622 5109.
E-mail address: t.nyokong@ru.ac.za (T. Nyokong).

0039-9140/$ – see front matter © 2011 Elsevier B.V. All rights reserved.
doi:10.1016/j.talanta.2011.07.069

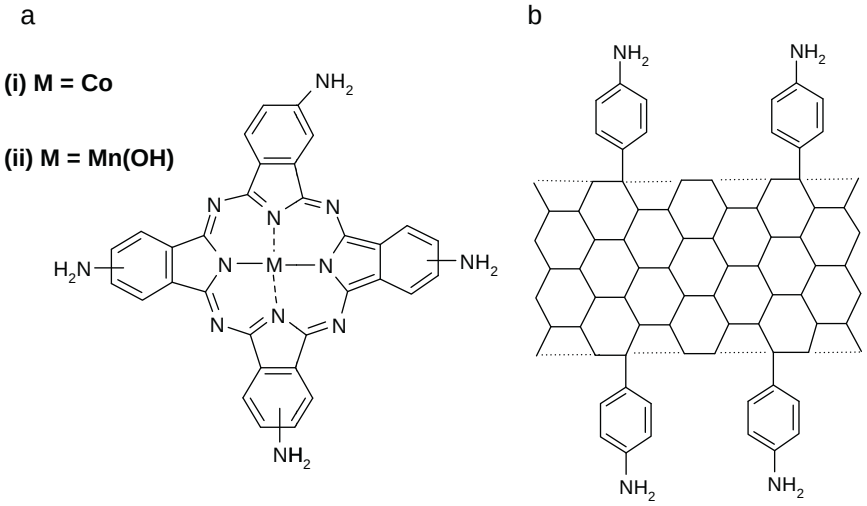

Fig. 1. Materials used in this study: (a) metallo-phthalocyanine (i) CoTAPc and (i) Mn(OH)TAPc and (b) phenyl-amine functionalized carbon nanotubes.

As an extension of our previous work [3], we investigate here the effect that carbon nanotubes will have on the electrocatalysis of H_2O_2 by MTAPc complexes (CoTAPc and MnTAPc). Phenyl-amine functionalized singled-walled carbon nanotubes (PA-SWCNTs) were immobilized covalently onto the phenyl-amine pre-grafted and benzene-1,4-dicarbaldehyde activated screen-printed gold electrode (SPAuE). CoTAPc and MnTAPc complexes were immobilized onto PA-SWCNT functionalized substrates to form hybrids, which were then studied for their electrocatalytic properties towards the detection of H_2O_2. Fig. 1 shows the structures of (a) MTAPc complexes containing (i) cobalt (CoTAPc) and (ii) manganese (MnTAPc) as metal ion centres, and (b) PA-SWCNT.

2. Experimental

2.1. Materials and suppliers

Single-walled carbon nanotubes (SWCNTs, 0.7–1.4 nm diameter, >90% carbon content and of it ≥77% carbon as SWCNT), N,N-dimethylformamide (DMF), benzene-1,4-dicarbaldehyde (BDCA), tetrabutylammonium tetrafluoroborate ($TBABF_4$), 4-nitrobenzene diazonium tetrafluoroborate (4-NBD) and absolute ethanol (EtOH) were purchased from Sigma–Aldrich and used as received. H_2O_2 (30%) was purchased from SAARChem. Ultra-pure water was obtained from a Milli-Q water system (Millipore Corp. Bedford, MA, USA) and was used throughout the experiments. Acetonitrile (ACN), phosphate salts (NaH_2PO_4 and Na_2HPO_4), ferricyanide $\{K_3[Fe(CN)_6]\}$ and ferrocyanide $\{K_4[Fe(CN)_6]\}$ were purchased from ACE Chemicals. The phosphate salts were used to prepare phosphate buffer solutions. Solutions in the electrochemical cell were de-aerated by bubbling argon prior to every experiment and the electrochemical cell was kept under argon atmosphere. Side wall functionalization of SWCNTs with phenyl-amine group was achieved using the reported method [6,9]. Manganese and cobalt tetra-amino phthalocyanine (Mn^{III}(OH)TAPc and CoTAPc) complexes were synthesized according to the published method [10,11].

2.2. Equipment

All electrochemical and impedance spectroscopy experiments were carried out using a computer-controlled Autolab Potentiostat/Galvanostat PGSTAT 302N purchased from EcoChemie (Utrecht, The Netherlands) driven by the General Purpose Electrochemical Systems data processing software (GPES software for electrochemistry) and FRA for impedance measurements and analysis. The electrochemical data was collected using screen-printed gold electrodes, SPAuE (C223AT purchased from Dropsens, Oviedo, Spain) with three electronic contacts for gold (Au, $r = 0.8$ mm) as working electrode, gold as counter electrode and silver|silver chloride (Ag|AgCl) as a reference electrode. Electrochemical impedance spectroscopy (EIS) experiments were recorded in the frequency range between 10 kHz and 100 MHz at the half-wave potential ($E_{1/2}$) of $[Fe(CN)_6]^{3-/4-}$ redox couple for bare and modified SPAuE with an amplitude of 5 mV rms sinusoidal modulation. The scanning electron microscopy (SEM) topography images of the bare and modified gold surfaces were obtained using the gold coated quartz crystals (AuCQC, 5 MHz, O100RX1) purchased from Stanford Research Systems (SRS). The AuCQC surfaces are smooth compared to SPAuE under SEM making surface differences due to modification easier to observe than on the rough SPAuE. The high resolution SEM (HRSEM) images were acquired using Nova NanoSEM 200 from FEI with X-ray microanalysis module for energy dispersive X-ray spectroscopy (EDS) measurements. The transmission electron microscopy (TEM) images were acquired using JEOL 2100F equipment and the copper grit coated with the materials of interest. Raman spectra for powder samples in KBr mixture were acquired using Thermo Nicolet Nexus 6700 FT-Raman spectrometer, with Nd:YAG laser 1064 nm. Surface-enhanced Raman spectra (SERS) were obtained using the Bruker Vertex 70-Ram II spectrometer equipped with a 1064 nm Nd:YAG laser and a liquid nitrogen cooled germanium detector.

2.3. Electrode modification

Prior to electrode modification, the SPAuEs were rinsed in ethanol solution and conditioned in sulfuric acid (0.5 M H_2SO_4) until reproducible scans were observed. The electrode was rinsed with ethanol solution and the modification of SPAuE was followed as illustrated in Scheme 1.

Step (i): electrochemical grafting of 4-NBD (1.0 mmol L^{-1}) in ACN solution containing 1 mmol L^{-1} $TBABF_4$ forming phenyl-nitro monolayer (5 cycles). The phenyl-nitro group was electrochemically reduced to form phenyl-amino (PA) monolayer by cycling in ethanol/water (1/9) solution containing 0.1 mol L^{-1} KCl.
Step (ii): activation of PA functionalized SPAuEs by immersing in the ethanol solution of BDCA for 4 h, exposing the other aldehyde

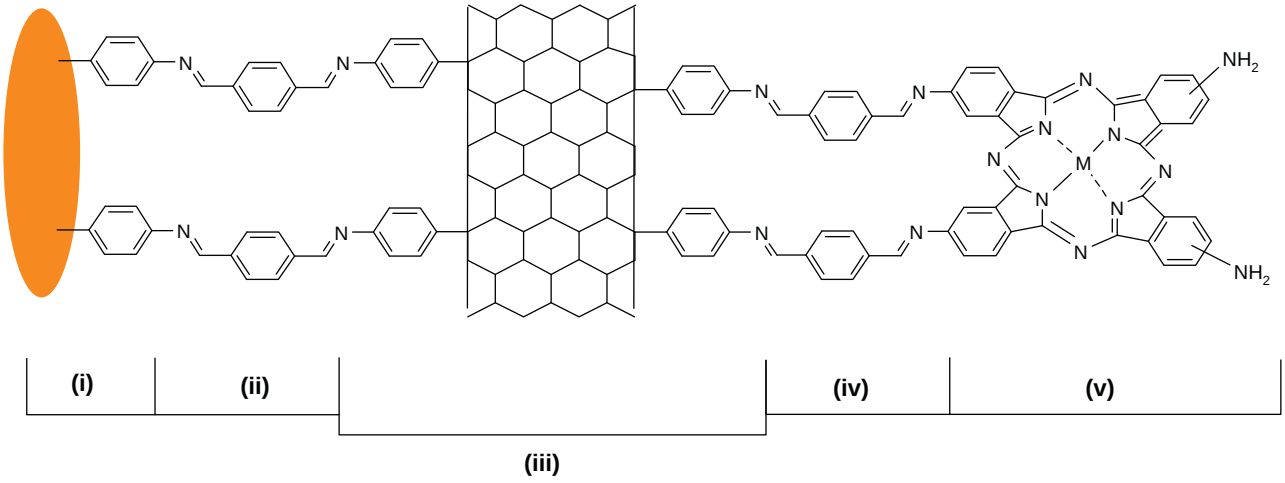

Scheme 1. The immobilization PA-SWCNT and MTAPc (M = Co or Mn) onto phenyl-amine grafted SPAuE. Step (i): electrochemical grafting of 4-NBD in ACN solution containing $TBABF_4$ and reduction of NO_2 group to form NH_2 (aprotic solution). Step (ii): activation of the amino group using BDCA ethanol solution. Step (iii): immobilization of PA-SWCNT (5%, w/w) in DMF. Step (iv) activation in BDCA mixed solution DMF/ethanol (1:1, v/v) and (v) immobilization of MTAPc in DMF.

group for further reaction with the amino groups from MTAPc and/or PA-SWCNT.
Step (iii): immobilization of PA-SWCNT by immersing the BDCA activated electrode into the PA-SWCNT in DMF solution for 4 h.
Step (iv): activation of the immobilized PA-SWCNT by immersing the PA-SWCNT functionalized surface into a BDCA in DMF/ethanol solution.
Step (v): immobilization of CoTAPc and MnTAPc complexes by immersing the BDCA activated PA-SWCNT electrode into an MTAPc DMF solution.

The bare and modified SPAuE surfaces using the procedure described in Scheme 1 are from here onwards represented as SPAuE (bare or unmodified), SPAuE–PA, SPAuE–PA-SWCNT, SPAuE–PA-SWCNT–MnTAPc and SPAuE–PA-SWCNT–CoTAPc.

For SEM measurements, the gold coated quartz crystals (AuCQC) were modified using similar protocol as the SPAuEs and are represented as AuCQC (bare), AuCQC–PA, AuCQC–PA-SWCNT, AuCQC–PA-SWCNT–MnTAPc and AuCQC–PA-SWCNT–CoTAPc.

3. Results and discussion

Fig. 2 shows the TEM images of (a) CoTAPc, (b) MnTAPc and (c) PA-SWCNT after the materials were initially dispersed in DMF solution through ultra-sonication followed by solvent evaporation on a copper grit. The CoTAPc TEM image in Fig. 2(a) showed high intermolecular aggregation and this aggregation was less visible on the MnTAPc TEM image in Fig. 2(b). The difference in the TEM images is due to that MnTAPc has an –OH axial ligand (Mn(OH)TAPc) which reduces intermolecular aggregation. The TEM image of PA-SWCNT in Fig. 2(c) showed a well dispersed PA-SWCNTs with diameter ranging from 0.7 to 10 nm. The original diameter for the SWCNT not functionalized as per the supplier information is 0.7–1.4 nm, therefore the increase in diameter of up to 10 nm shows that the functionalization of the SWCNT with phenyl-amine group has occurred. This increase in SWCNT diameter could be attributed to (i) the nanotubes intertwined together or (ii) dual functionalization of the benzene-1,4-diamine forming a benzene-1,4-*bis*-diazonium (N_2^+) on both amine groups leading to two or more SWCNT linked and forming a polymeric SWCNT conjugate.

The immobilization of MTAPc and their electrocatalytic activity towards reduction of H_2O_2 has been recently reported [3] and in this work the PA-SWCNT and MTAPc immobilization are investigated following the method outlined in Scheme 1. This method yielded a very stable carbon nanotubes and phthalocyanine monolayer on the gold electrode surface owing to their covalent attachment. The order in which the metallo-phthalocyanine complexes and carbon nanotubes are immobilized onto gold electrode surface has an impact on the electron-transfer and electrocatalysis [12]. In the reported work [12], the authors found better electrocat-

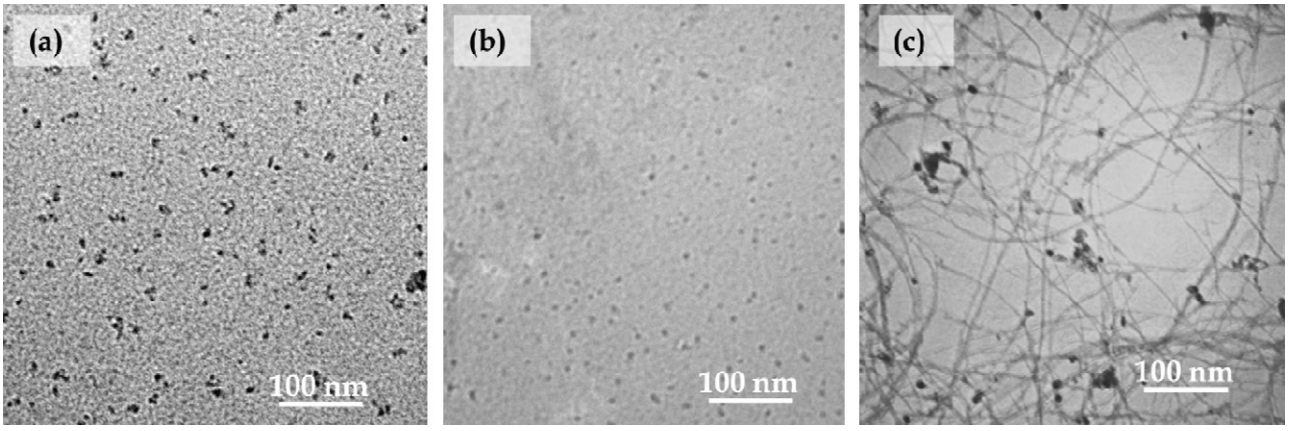

Fig. 2. TEM images of (a) CoTAPc, (b) MnTAPc and (c) PA-SWCNT dispersed in DMF and modified onto mesh copper grit with solvent evaporated.

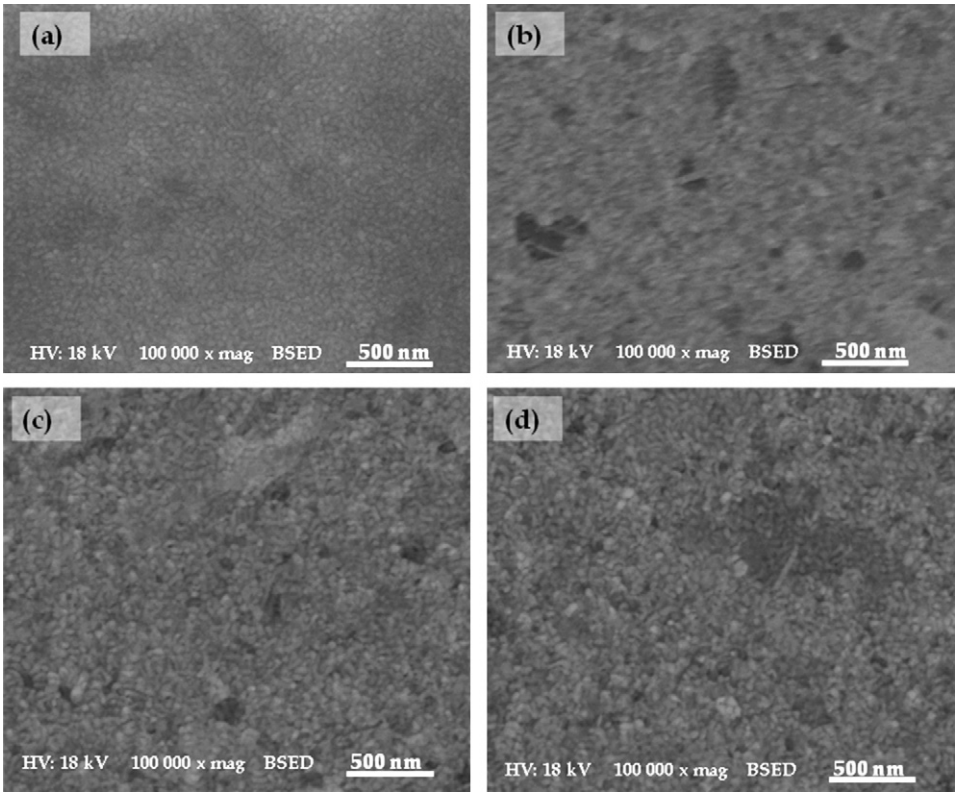

Fig. 3. HRSEM images for (a) bare AuCQC, (b) AuCQC–PA-SWCNT, (c) AuCQC–PA-SWCNT–MnTAPc and (d) AuCQC–PA-SWCNT–CoTAPc surfaces.

alytic properties when nanostructured iron phthalocyanines were immobilized on top of the carbon nanotubes. Therefore, the immobilization of MTAPc complexes will be at the layer exposed to the solution, i.e. at the electrode–solution interface. This immobilization of MTAPc complexes on top of the PA-SWCNT is important because the metal ion centres from MTAPc complexes contribute to the overall mechanism for H_2O_2 electrocatalysis [3,4]. The formation of Schiff-base product using BDCA as a cross linker has been reported before for the formation of the heterobinuclear porphyrin dimers [13]. The choice of using BDCA as a cross-linker allows for the extension of the electronic delocalization of the PA-SWCNT and MTAPc complexes as observed before [3]. This extension of electronic delocalization at PA-SWCNT is intended to promote and retain the good conducting or electron-transfer properties of SWCNTs. At the immobilized MTAPc complexes, the extension of electronic delocalization is expected to lower the reduction potential and increase their electrocatalytic activity. This lowering of potential, influenced by delocalization, has been reported before for the conjugated porphyrin complexes [14]. Therefore, the SWCNT–MTAPc hybrids are expected to have enhanced electrocatalytic properties due to the synergistic effect expected when the two materials act together.

3.1. Microscopic and spectroscopic surface characterization

The HRSEM characterization of the electrode modified with PA-SWCNT and MTAPc complexes was carried out. Fig. S1 (supporting information) shows that the bare AuCQC is smoother than the bare SPAuE. Therefore, the use of AuCQC will enhance and make visible the surface modification changes with monolayer thin films than on the rough SPAuE. Fig. 3 shows HRSEM images of (a) bare AuCQC, (b) AuCQC–PA-SWCNT, (c) AuCQC–PA-SWCNT–MnTAPc and (d) AuCQC–PA-SWCNT–CoTAPc electrodes modified following the procedure in Scheme 1. From the HRSEM images, it is clear that electrode modification indeed took place as the morphology of these images was different, especially between the bare (AuCQC) in Fig. 3(a) and AuCQC–PA-SWCNT in Fig. 3(b) which showed a dense film of PA-SWCNT deposited. The film was even thicker when MnTAPc in Fig. 3(c) and CoTAPc in Fig. 3(d) were immobilized, confirming the attachment of MTAPc complexes onto PA-SWCNT functionalized gold surface.

The EDS analysis of the bare and modified surfaces further confirmed the surface modifications with PA-SWCNT and the MTAPc (MnTAPc and CoTAPc) for the formation of SWCNT–MTAPc hybrid sensing layer. Fig. 4 shows EDS spectra of (a) bare AuCQC, (b) AuCQC–PA-SWCNT and (c) AuCQC–PA-SWCNT–CoTAPc. At bare AuCQC in Fig. 4(a) we observed a dominating gold M peaks (Au-M) and this was expected as gold was used as the substrate in this study. The residues due to carbon (C–K peak) and nitrogen (N–K peak) were also observed but in very smaller quantities. The gold surface was modified with PA to form AuCQC–PA monolayer modified surface (image not shown) and the EDS spectrum of this electrode showed a slight increase in carbon (C–K) peaks when compared to that of bare AuCQC surface (Fig. 4a) and this was attributed to a very thin PA monolayer. There was a significant increase in the C–K peak after modifying the surface with PA-SWCNT, Fig. 4(b). The increase in the C–K peak is attributed to the presence of the highly carbon-based material (PA-SWCNT) immobilized onto the AuCQC surface forming an AuCQC–PA-SWCNT. As the C–K peak increased, the Au–M peak intensity decreased, signifying the coverage of gold surface with PA-SWCNT. Table 1 shows the weight percentage of elements found on the gold surfaces. CoTAPc complex was immobilized onto PA-SWCNT surface to yield an AuCQC–PA-SWCNT–CoTAPc and the increase in C–K peak was also observed to be due to the attachment of CoTAPc, Fig. 4(c). The results obtained from the immobilization of MnTAPc were similar to those of CoTAPc. The other elements, oxygen (O–K) and nitrogen (N–K) did not show any reasonable increase or decrease before

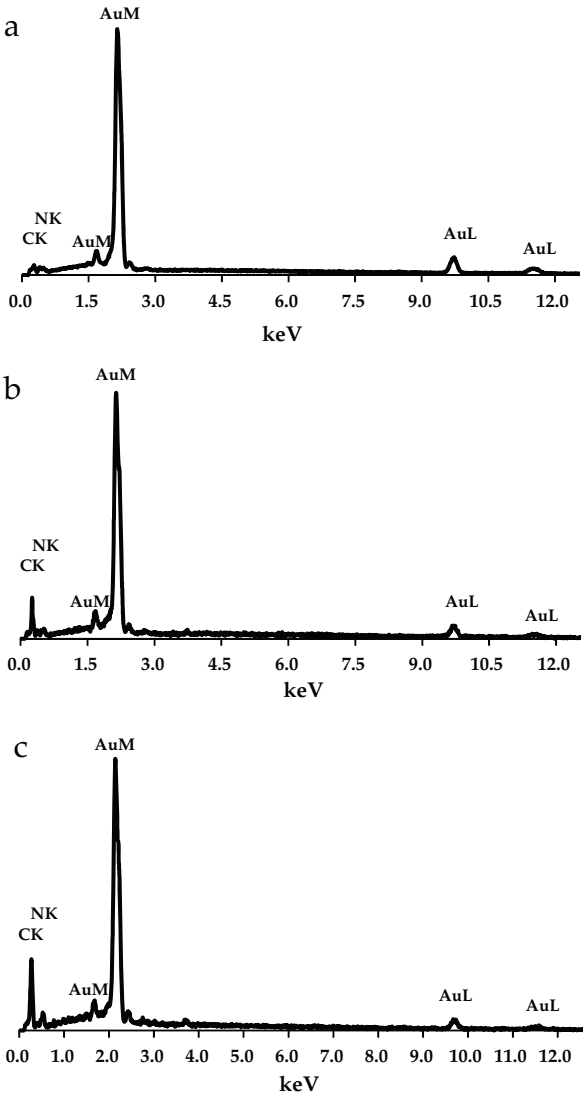

Fig. 4. Energy dispersive X-ray spectra for (a) AuCQC (bare), (b) AuCQC–PA-SWCNT and (c) AuCQC–PA-SWCNT–CoTAPc.

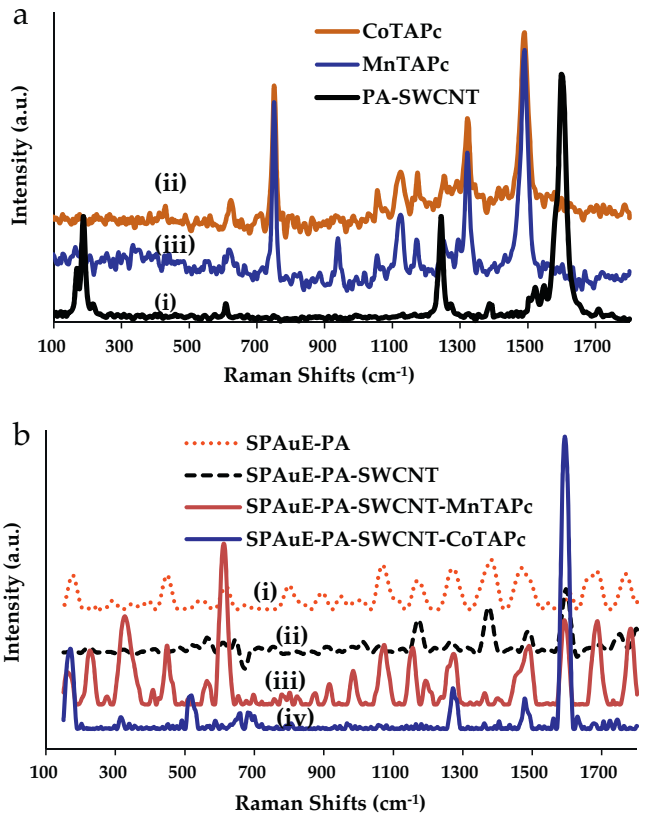

Fig. 5. (a) Raman spectra of PA-SWCNT, CoTAPc and MnTAPc in powder form. (b) Raman spectra of SPAuE modified surfaces (i) SPAuE–PA, (ii) SPAuE–PA-SWCNT, (iii) SPAuE–PA-SWCNT–MnTAPc and (iv) SPAuE–PA-SWCNT–CoTAPc.

and after modification. Therefore no conclusion could be drawn from the N–K and O–K peaks. It was interesting to note that at MTAPc modified surfaces, we could not see the metal ion peaks due to cobalt and manganese as has been previously reported [3]. This could be attributed to the high carbon content on the SWCNT present on the electrode surfaces, hence the metal ion peaks are very small and buried under other highly intense carbon, nitrogen and gold peaks. It is of interest to note that the presence of the immobilized SWCNT resulted in the non-aggregated immobilization of MTAPc complexes. The aggregation of the immobilized MTAPc complexes was observed in our previous studies [3]. The EDS results are summarized in Table 1, which shows the observed elements and their weight percentage (wt.%) at modified surfaces. As can be seen from Table 1, the weight percentage (wt.%) of carbon (C–K peak) increased with each immobilization of the carbonaceous material, i.e. PA, PA-SWCNT, CoTAPc and MnTAPc, while the gold weight percentage (wt.%) decreased. The other elements oxygen (O–K) and nitrogen (N–K) showed no trend with electrode modification. The results from EDS spectra and the elemental analysis clearly show the presence and the successful immobilization of PA, PA-SWCNT and MTAPc complexes (CoTAPc and MnTAPc) onto gold electrode surfaces. The AuCQC surfaces were used only for the SEM measurements, the following sections will investigate the surface modifications on screen-printed gold electrodes (SPAuE) for electrochemical measurements.

We further confirmed the surface modification and covalent immobilization of PA, PA-SWCNT and MTAPc (CoTAPc and MnTAPc) complexes using Raman spectroscopy. Fig. 5 shows (a) Raman spectra of (i) PA-SWCNT, (ii) CoTAPc and (iii) MnTAPc in powder form and (b) Raman spectra of SPAuE surfaces modified with (i) PA, (ii) PA-SWCNT, (iii) PA-SWCNT–MnTAPc and (iv) PA-SWCNT–CoTAPc. The Raman spectra of PA-SWCNT in Fig. 5(a)(i) showed Raman peaks at 1599 cm^{-1}, 1244 cm^{-1}, 187 cm^{-1} and 167 cm^{-1}, Table 2 The peak at 1599 cm^{-1} is a G-band and is observed at the simi-

Table 1
Elemental quantification, weight percentage (wt.%) for the elements obtained using EDS spectra of the bare and modified gold surfaces above.

Electrodes (elements)	AuCQC (wt.%)	AuCQC–PA (wt.%)	AuCQC–PA-SWCNT (wt.%)	AuCQC–PA-SWCNT–MnTAPc (wt.%)	AuCQC–PA-SWCNT–CoTAPc (wt.%)
Carbon (C–K peak)	4.96	8.54	21.45	31.56	31.46
Nitrogen (N–K peak)	3.78	2.53	2.36	4.11	3.56
Oxygen (O–K peak)	1.12	1.68	1.88	4.50	3.00
Gold (Au–L peak)	90.13	87.24	74.30	59.84	61.97

Table 2
Molecular vibrations of PA-SWCNT, CoTAPc and MnTAPc immobilized onto functionalized gold surface and the corresponding vibrations of the same materials in the powder form. The units for the Raman shift values within the table are cm^{-1}.

Powder			Modified SPAuE surfaces			Interpretation
PA-SWCNT	MnTAPc	CoTAPc	SPAuE–PA-SWCNT	SPAuE–PA-SWCNT–MnTAPc	SPAuE–PA-SWCNT–CoTAPc	
167, 187	–	–	–	168	171	RMB SWCNT
–	–	–	233	231	318	Au–C bending
–	–	–	–	332	–	Mn–O
–	–	–	571, 617	451, 590	519, 588	Au–C stretch
603	615, 750	619,750	659	613	681, 688	Ring deformation
–	940	–	–	920, 987	–	Out-of-plane bending
–	1055, 1120	1054, 1120	1016, 1174	1074, 1150	–	C–H bending
–	1171, 1252	1174, 1251	–	1197, 1277	1273	C–H bending
1244	–	–	1269	–	–	D-band
–	1321	1321	–	–	–	C–N breathing
1382	–	–	1377	–	–	C–N stretch
–	1491	1487	–	–	–	C=C pyrrole stretch
–	–	–	1495	–	1479	C=C stretch
1599	–	–	1600, 1755	1595, 1689	1595	G-band

lar positions to the reported Raman shifts [9,15] for SWCNT. The peak at 1244 cm^{-1} is a D-band for defective carbon network [9,15] confirming the sidewall functionalization of SWCNT with PA group and we also observed the split radial breathing mode (RBM) at 167 cm^{-1} and 187 cm^{-1} [9,15–18]. The MTAPc complexes (CoTAPc and MnTAPc) in Fig. 5(a)(ii and iii) showed Raman peaks similar to those reported for the phthalocyanine complexes [19,20]. The materials were immobilized onto SPAuE surfaces following the procedure in Scheme 1. Fig. 5(b) shows the Raman spectra of SPAuE modified surfaces. It is discernible, from the spectra in Fig. 5(b), that the surface modification indeed took place as the Raman peaks due to the immobilized materials (PA-SWCNT and MTAPc) were observed. The PA modified electrodes exhibited peaks which were similar to those observed at unmodified electrode (data not shown for the latter) and this was due to the fact that the PA is a very thin monolayer film and its effect is almost negligible. We have previously shown [3] that the PA could not effect visible change in surface morphology during SEM measurements. The immobilization of PA-SWCNT onto phenyl amine functionalized surface yielded a PA-SWCNT monolayer modified surface with Raman peaks at 1597 cm^{-1}, 1408 cm^{-1} and 1180 cm^{-1} (Table 2) which are characteristic of SWCNT G and D-bands. Further modification of the PA-SWCNT functionalized surfaces with CoTAPc and MnTAPc complexes resulted in the emergence of multiple peaks which are different from those of PA-SWCNT. The new peaks could be attributed to the presence of the MTAPc complexes and their immobilization onto PA-SWCNT modified surface. The peaks of interest which are different from G and D-bands from SWCNT were observed at 612 cm^{-1} (ring deformation), 1078–1280 cm^{-1} (C–H bending) and 1691 cm^{-1} (C=C pyrrole stretches) which are clearly visible at MnTAPc modified PA-SWCNT surface. These peaks are typical of phthalocyanine Raman shifts as previously observed at SAMs modified gold surface [19]. At CoTAPc modified surface the peaks due to phthalocyanine ring were also observed but were masked by the highly intense SWCNT G-band with only the traces of CoTAPc observed. The Raman surface measurements clearly confirmed the surface modifications shown in Scheme 1. The Raman measurements also confirm the observed surface morphology changes on the SEM and EDS analysis.

3.2. Electrochemical surface characterization

The electrochemical properties of the bare and modified electrodes were investigated using cyclic voltammetry and electrochemical impedance spectroscopy measurements (Nyquist representation). These experiments were also studied to further characterize the modified electrode surfaces using ferricyanide $[Fe(CN)_6]^{3-/4-}$ as a redox probe in solution. Fig. 6 shows the (a) cyclic voltammograms (CV) and (b) Nyquist plots of (i) bare SPAuE, (ii) SPAuE–PA, (iii) SPAuE–PA-SWCNT, (iv) SPAuE–PA-SWCNT–MnTAPc and (v) SPAuE–PA-SWCNT–CoTAPc in (1:1) 2.0 mmol L^{-1} $K_4/K_3Fe(CN)_6$ in 0.10 mol L^{-1} KCl.

The cyclic voltammograms of the bare gold screen-printed electrode in Fig. 6(a)(i) shows the reversible redox couple due to $[Fe(CN)_6]^{3-/4-}$ with the peak-to-peak separation (ΔE) of 81 mV, Table 3. Upon modifying the electrodes with the phenyl-amino group, in Fig. 6(a)(ii) ΔE increased to about 90 mV and this is attributed to the insulating layer of phenyl-amino that has formed on the electrode surfaces. Also at phenyl-amino monolayer, the redox peak due to $[Fe(CN)_6]^{3-/4-}$ shifted to less positive potential, clearly confirming the presence of PA monolayer on the electrode surface and that this redox process was not inhibited. Further

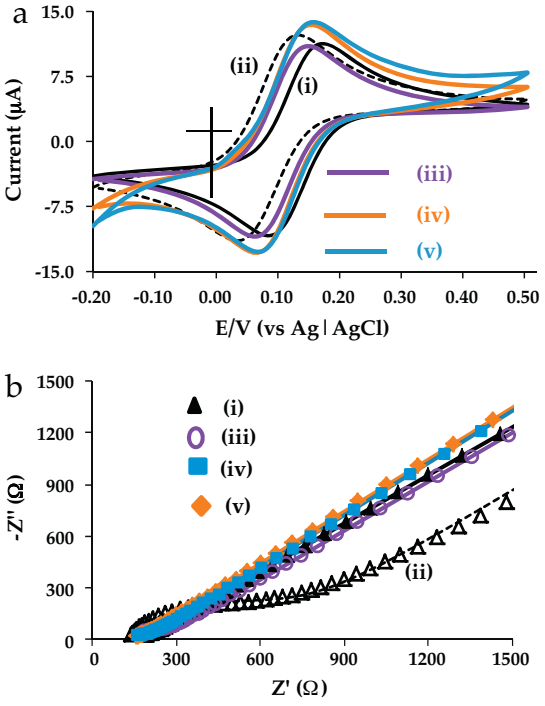

Fig. 6. (a) CVs and (b) Nyquist plots of (i) bare SPAuE, (ii) SPAuE–PA, (iii) SPAuE–PA-SWCNT, (iv) SPAuE–PA-SWCNT–MnTAPc and (v) SPAuE–PA-SWCNT–CoTAPc in (1:1) 2.0 mmol L^{-1} $K_4/K_3Fe(CN)_6$ in 0.10 mol L^{-1} KCl.

Table 3
The summary of parameters obtained from cyclic voltammetry and electrochemical impedance spectroscopy experiments in $Fe(CN)_6^{3-/4-}$ solution.

Electrodes	R_S (kΩ cm^{-2})	R_{CT} (kΩ cm^{-2})	n	Q (μF cm^{-2})	ΔE (mV)	k_{app} (10^{-4} cm s^{-1})
SPAuE[a]	4.72	1.79	0.87	56	81	1.20
SPAuE–PA[a]	4.12	43.67	0.88	94	90	0.049
SPAuE–PA-SWCNT	5.38	3.07	0.90	31	80	0.70
SPAuE–PA-SWCNT–MnTAPc	4.62	0.88	0.85	85	80	2.44
SPAuE–PA-SWCNT–CoTAPc	4.52	1.76	0.87	143	80	1.22
SPAuE–PA–CoTAPc[a]	4.43	9.66	0.92	22	80	0.22
SPAuE–PA–MnTAPc[a]	4.32	9.69	0.94	22	80	0.22

[a] Values added for comparison and were obtained from Ref. [3].

modification of the electrodes with PA-SWCNT in Fig. 6(a)(iii) showed that the reversibility was restored, ΔE (80 mV); to almost similar to that of the bare (81 mV) and much less than that for phenyl-amino monolayer (90 mV) modified electrodes, Table 3. The immobilization of MTAPc complexes onto electrodes modified with PA-SWCNT, shown in Fig. 6(a)(iv and v) yielded similar ΔE values to that of carbon nanotubes modified electrodes. The $[Fe(CN)_6]^{3-/4-}$ redox peak currents increased at PA-SWCNT–MTAPc modified gold surfaces clearly indicating the good conducting properties of the hybrid monolayer.

Electrochemical impedance spectroscopy (EIS) measurements in $[Fe(CN)_6]^{3-/4-}$ solution were investigated to assess the electron-transfer properties of the modified gold surfaces. Fig. 6(b) shows a Nyquist plots for (i) SPAuE, (ii) SPAuE–PA, (iii) SPAuE–PA-SWCNT, (iv) SPAuE–PA-SWCNT–MnTAPc and (v) SPAuE–PA-SWCNT–CoTAPc surfaces. The Nyquist plot data was fitted using Randle's equivalent circuit which has two regions of interest, i.e. high frequency region (electron-transfer properties) and low frequency region (electrolyte diffusion controlled properties). The region of interest to this work is the high frequency region which is the kinetically controlled region and will give us the kinetics of the modified gold surfaces. Kinetically controlled region in the Nyquist plot is of high importance since it shows the semi-circle which is related to the charge-transfer resistance (R_{CT}). The smaller the R_{CT}, the more conducting the electrode or the materials used to modify the electrode. Fig. 6(b)(i) for bare SPAuE shows the small semi-circle which increases after modifying the electrodes with the PA monolayers, Fig. 6(b)(ii). The data was fitted using the Randle's equivalent circuit and the obtained data parameters after fitting are shown in Table 3. The R_{CT} value for a bare electrode surface was 1.79 kΩ cm^{-2} and this value was 43.67 kΩ cm^{-2} on SPAuE–PA, 3.07 kΩ cm^{-2} on SPAuE–PA-SWCNT, 0.88 kΩ cm^{-2} on SPAuE–PA-SWCNT–MnTAPc and 1.76 kΩ cm^{-2} on SPAuE–PA-SWCNT–CoTAPc. The R_{CT} values showed an increase at SPAuE–PA and SPAuE–PA-SWCNT compared to bare SPAuE, and a decrease at SPAuE–PA-SWCNT–MnTAPc and SPAuE–PA-SWCNT–CoTAPc surfaces. The R_{CT} value was the smallest at SPAuE–PA-SWCNT–MnTAPc compared to all other electrodes. The decrease in R_{CT} values at PA-SWCNT–MTAPc is attributed to (i) SWCNTs being a good conductor of electrons [12,21] and (ii) the combination of the two electrocatalytically active materials (SWCNT and MTAPcs) having synergistic effects in terms of enhancing electron transfer to and from the electrode surface. It was interesting to note that the R_{CT} values decreased for SPAuE–PA-SWCNT (3.07 kΩ cm^{-2}) and SPAuE–PA-SWCNT–MTAPc (1.76 kΩ cm^{-2} and 0.88 kΩ cm^{-2}) complexes when compared to that of SPAuE–PA electrode (43.67 kΩ cm^{-2}). The values of PA-SWCNT–MTAPc modified gold surfaces were much less than those of PA–MTAPc modified gold surfaces recently reported [3] and shown in Table 3.

The apparent electron-transfer rate constant (k_{app}) was obtained from the conventional Eq. (1) [21,22]. The redox probe $[Fe(CN)_6]^{3-/4-}$ and the R_{CT} values obtained in Table 3, were used to calculate the k_{app} from Eq. (1). This method investigates the outer sphere kinetic properties of the immobilized thin films and their interaction with the redox probe in solution.

$$k_{app} \approx k^0 = \frac{RT}{n^2F^2AR_{CT}c} \quad (1)$$

where c is a concentration of $[Fe(CN)_6]^{3-/4-}$ (2 mmol L^{-1}), R_{CT} (charge transfer resistance from fitted data in Table 3), A is the real area of the gold electrode (0.0352 cm^2), n = 1 (electron involved in the $[Fe(CN)_6]^{-3/-4}$ redox process), with R, T and F have their usual meaning. The bare gold electrode surface gave the k_{app} value of 1.20×10^{-4} cm s^{-1}. The electron transfer properties at unmodified surface are mainly controlled by the diffusion of the solution ions to the surface which at bare electrode surface the solution ions are unhindered. The apparent electron transfer rate constants at SPAuE–PA, and SPAuE–PA–MTAPcs were low with the values 0.049×10^{-4} cm s^{-1} and to 0.22×10^{-4} cm s^{-1} for these surfaces, respectively, compared to SPAuE. The decrease in k_{app} values is attributed monolayer coverage on the electrode surface thus blocking the solution ions from reaching the surface. The solution blocking effect was worse on the PA modified surface (0.049×10^{-4} cm s^{-1}). When MTAPc complexes are immobilized onto SPAuE–PA surfaces, forming PA–MTAPc monolayers, the k_{app} values increased to 0.22×10^{-4} cm s^{-1} compared to PA alone. The increase from 0.049×10^{-4} cm s^{-1} (SPAuE–PA) to 0.22×10^{-4} cm s^{-1} for PA–MTAPc could be attributed to the conducting and electrocatalytic properties of MTAPc complexes. The electrode when modified with PA-SWCNT gave the k_{app} value of 0.70×10^{-4} cm s^{-1}. The increase in k_{app} value at PA-SWCNT could be attributed to the SWCNT being a good conductor of electrons. SWCNT are metallic in their nature [16], hence the electrode sees a continuation of its metallic properties. The k_{app} value for PA-SWCNT of 0.70×10^{-4} cm s^{-1} is still less than that of bare gold surface (1.20×10^{-4} cm s^{-1}) and this is due to the fact that SWCNTs are carbon-based materials compared to pure gold metal. There was a significant increase in the k_{app} values at SPAuE–PA-SWCNT–MnTAPc (2.44×10^{-4} cm s^{-1}) and SPAuE–PA-SWCNT–CoTAPc (1.22×10^{-4} cm s^{-1}) even better than that of bare SPAuE (1.20×10^{-4} cm s^{-1}). The observed increase k_{app} values could be attributed to the synergistic effect of the conducting and electrocatalytic SWCNT and MTAPc hybrids. The SWCNTs clearly have additional advantages when immobilized on the electrode surface and when combined with the electrocatalytic MTAPc complexes. The combination of the two materials clearly shows an increase in the apparent electron transfer rate constants. Other parameters obtained from fitting the data are summarized in Table 3. The R_S (solution resistance) did not change with electrode modification. This is expected, since electrode modification does not significantly affect this parameter.

The Q (double-layer capacitance) varied with the surface modification but there was no well-defined trend to attribute the capacitance variation to the electrode modification. The n values (where n is an exponent-related to depression angle [21]) are important to mention as they give information about the behaviour of bare and modified electrode surfaces. If the electrode or modi-

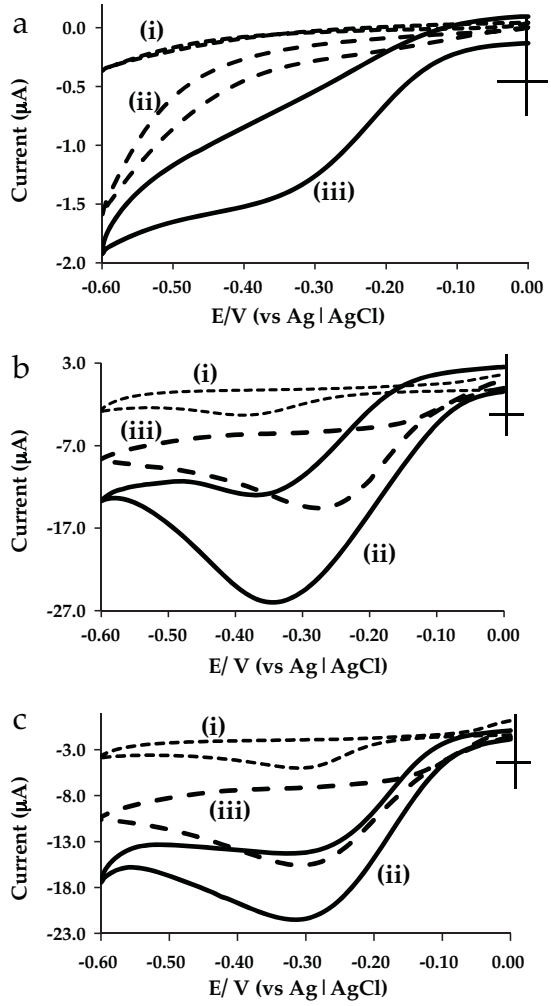

Fig. 7. CVs of (a) 1.0 mmol L^{-1} H_2O_2 in pH 7.4 on (i) SPAuE, (ii) SPAuE–PA, and (iii) SPAuE–PA-SWCNT; (b) SPAuE–PA-SWCNT–MnTAPc in (i) pH 7.4 and (ii) 1.0 mmol L^{-1} H_2O_2 and (iii) SPAuE–PA–MnTAPc in 1.0 mmol L^{-1} H_2O_2; and (c) SPAuE–PA-SWCNT–CoTAPc in (i) pH 7.4 and (ii) 1.0 mmol L^{-1} H_2O_2 and (iii) SPAuE–PA–CoTAPc in 1.0 mmol L^{-1} H_2O_2.

fied electrode behaves like a pure resistor ($n = 0$), Warburg diffusion ($n = 0.5$) and pure capacitor ($n = 1$). The n values ranges from 0.85 to 0.94 and these values are all close to unity (=1) indicating that the electrode behaves like a capacitor.

3.3. Electrocatalysis of H_2O_2 at SPAuE–PA-SWCNT–MTAPc

The electrocatalytic properties of the PA-SWCNT and MTAPc hybrid modified screen-printed gold electrodes were investigated for the detection of H_2O_2 in physiological conditions (pH 7.4). Fig. 7(a) shows the electro-reduction of 1.0 mmol L^{-1} H_2O_2 in pH 7.4 for (i) SPAuE, (ii) SPAuE–PA and (iii) SPAuE–PA-SWCNT; (b)(i) SPAuE–PA-SWCNT–MnTAPc in pH 7.4, (ii) SPAuE–PA-SWCNT–MnTAPc and (iii) SPAuE–PA–MnTAPc in 1.0 mmol L^{-1} H_2O_2; (c)(i) SPAuE–PA-SWCNT–CoTAPc in pH 7.4, (ii) SPAuE–PA-SWCNT–CoTAPc and (iii) SPAuE–PA–CoTAPc in 1.0 mmol L^{-1} H_2O_2. At SPAuE and SPAuE–PA, surfaces in Fig. 7(a), there was no well-defined electrocatalytic peak observed due to H_2O_2 electrocatalysis only the increase in currents was observed. The SPAuE–PA-SWCNT surface showed further increase in currents confirming the conducting properties of SWCNT. In Fig. 7(b and c)(i) pH 7.4 buffer alone, the PA-SWCNT–MTAPc modified electrodes showed the reduction peaks at −0.35 V and −0.32 V for SPAuE–PA-SWCNT–MnTAPc and SPAuE–PA-SWCNT–CoTAPc, respectively. The observed reduction peaks are due to Mn^{III}/Mn^{II} and Co^{II}/Co^{I}, respectively. The surface concentrations or coverages ($\Gamma_{PA\text{-}SWCNT\text{–}MTAPc}$) for modified surfaces were calculated by integrating the charge under the reduction peaks due to the metal ions using Eq. (2).

$$\Gamma_{PA\text{-}SWCNT\text{–}MTAPc} = \frac{Q}{nFA} \quad (2)$$

where Q is the background corrected charge under the metal reduction peak (Coulombs), n is the number of electrons transferred (=1), F is a faraday's constant (96,485 Coulombs mol^{-1}) and A is the real area (0.0352 cm^{-2}) of the electrode as obtained in our previous study [3]. The surface coverage values calculated from Eq. (2) using the real surface area were found to be 1.60×10^{-9} mol cm^{-2} for SPAuE–PA-SWCNT–MnTAPc and 2.68×10^{-9} mol cm^{-2} for SPAuE–PA-SWCNT–CoTAPc. The surface coverage values were higher than 1.0×10^{-10} mol cm^{-2} for a phthalocyanine ring lying flat on the electrodes surface [23] leading to the conclusion that the phthalocyanine complexes assume a perpendicular orientation. The surface coverage values were slightly higher than the values previously reported [3] for phthalocyanine molecules attached to the PA monolayer. This increase in surface coverage indicates an increase in surface area due to the immobilized PA-SWCNT allowing for more MTAPc complexes to be covalently attached onto the electrode surface.

The electrocatalytic behaviour was observed for MTAPc modified electrodes, Fig. 7(b and c)(ii and iii) towards 1.0 mmol L^{-1} H_2O_2 in pH 7.4. The electrocatalytic peak due to 1.0 mmol L^{-1} H_2O_2 at PA–MTAPc modified SPAuE surfaces, Fig. 7(b and c)(iii), was observed at −0.31 V and −0.28 V for CoTAPc and MnTAPc, respectively. The enhancement in the electrocatalytic peak current due to 1.0 mmol L^{-1} H_2O_2 was observed at SPAuE–PA-SWCNT–MTAPc modified electrodes in Fig. 7(b and c)(ii) compared to MTAPc modified electrodes (SPAuE–PA–MTAPc) in Fig. 7(b and c)(iii). The enhancement in peak current at SPAuE–PA-SWCNT–MTAPc electrodes was attributed to the immobilized PA-SWCNTs being good in shuttling and amplifying electrons between the MTAPc electrocatalytic sites and the electrode surface. The electrocatalytic peaks due to electro-reduction of 1.0 mmol L^{-1} H_2O_2 were observed at −0.38 V for SPAuE–PA-SWCNT–MnTAPc and −0.30 V for SPAuE–PA-SWCNT–CoTAPc. The electro-reduction peaks of H_2O_2 appeared close to where the metal reduction peaks occurred clearly showing the involvement of the phthalocyanine central metal ions in the electrocatalytic process [3,4] even in the presence of PA-SWCNT. Fig. S2 (supporting information) shows the proposed mechanism by which the electrocatalytic process takes place on the PA-SWCNT–MTAPc modified surface. The conversion of H_2O_2 to water and oxygen is catalysed by the central metal in MPc complexes. The electrocatalytic peak currents for SPAuE–PA-SWCNT–MTAPc electrodes in the presence of 1.0 mmol L^{-1} H_2O_2, in Fig. 7(b and c)(ii), were higher than those of SPAuE–PA-SWCNT in Fig. 7(a)(iii) and SPAuE–PA–MTAPc in Fig. 7(b and c)(iii). The increase in current clearly indicates the efficiency of PA-SWCNT as a good electron conductors resulting in signal amplification. The alternative immobilization where MTAPc are immobilized first and the PA-SWCNT on top were not investigated and this is due to the results of the reported study [12]. This study showed that immobilizing SWCNTs on top of electrocatalytic MPc complexes resulted in the decrease in the electrocatalytic signal as compared to when the MPc complexes are at the electrode–solution interface. Therefore, the MTAPc complexes participate in the electrocatalytic reduction mechanism of H_2O_2 while SWCNTs assist in the communication (i.e. relay and amplify transferred electrons) between the electrode and the electrocatalytic site.

Table 4
Electroanalytical properties of electrodes modified with PA–MTAPc and PA-SWCNT–MTAPc in varied concentrations of H_2O_2 and at different electrocatalytic peak potentials.

Electrodes	LoD (10^{-7} mol L^{-1})	LCR (μmol L^{-1})	Sensitivity (mA mmol L^{-1} cm^{-2})	E_p, H_2O_2 (V)	$E_{1/2}$, M_{red} (V)
SPAuE–PA–MnTAPc	1.17	1.0–30.0	0.15	−0.28	−0.30
SPAuE–PA-SWCNT–MnTAPc	4.42	1.0–30.0	2.79	−0.38	−0.35
SPAuE–PA–CoTAPc	5.82	1.0–30.0	0.19	−0.31	−0.24
SPAuE–PA-SWCNT–CoTAPc	6.43	1.0–30.0	5.16	−0.30	−0.32

LoD: limit of detection; LCR: linear concentration range; E_p: electrocatalytic peak potential; $E_{1/2}$: half-wave potential and M_{red}: metal ion reduction couple.

3.4. Electroanalysis of H_2O_2 at PA–MTAPc and PA-SWCNT–MTAPc SPAuEs

The electroanalytical properties of SPAuE electrodes modified with PA–MTAPcs and PA-SWCNT–MTAPcs towards H_2O_2 were studied using chronoamperometry method [6]. Fig. 8 shows (a) amperometric response at varied H_2O_2 concentrations ranging from 1.0 to 30 μmol L^{-1} at SPAuE–PA-SWCNT–MnTAPc and calibration curves of steady-state current (I_{SS}) versus H_2O_2 concentration [H_2O_2] for (b) SPAuE–PA–MTAPc and (c) SPAuE–PA-SWCNT–MTAPc, M = Mn (i) and Co (ii). At the applied potential (E_{app}) of −0.38 V, the increase in [H_2O_2] resulted in a negative increase in steady-state catalytic currents, typical of electrocatalytic reduction using SPAuE–PA-SWCNT–MnTAPc as an example in Fig. 8(a). The negative increase in I_{SS} was linearly related to the increase in H_2O_2 concentrations, Fig. 8(b) and (c) for the studied electrodes. The chronoamperometry results obtained for other electrodes were similar to that of SPAuE–PA-SWCNT–MnTAPc in Fig. 8(a) at their respective applied potentials (Table 4). The limit of detection for the PA-SWCNT–MTAPc and PA–MTAPc modified electrodes were of the orders of 10^{-7} mol L^{-1} using the 3δ notation. The modified electrodes gave good linear calibration curves for H_2O_2 concentrations ranging from 1.0 to 30.0 μmol L^{-1}. The sensitivity of these electrodes ranged from 0.15 to 5.16 mA mmol L^{-1} cm^{-2} with the PA-SWCNT–MTAPc modified SPAuEs showing better sensitivity compared to PA–MTAPc modified SPAuEs. The analytical parameters obtained from the experiments in Fig. 8 are summarized in Table 4. The limit of detection (LoD) values obtained in this work were much less than those obtained for the gold electrode modified with SWCNTs-nano FePc using a layer-by-layer self-assembly monolayer method [12]. These LoD values are comparable to the gold electrode surfaces modified MPc polymers [4] and self-assembled monolayers of MPc [24,25] but less than those obtained for HRP (horse-radish peroxidase) modified gold electrodes [26–28]. The results obtained show that the electrodes can potentially be used for the analysis of H_2O_2 and the calibration curves will allow for unknown sample analysis. The use of screen-printed gold electrodes further shows the possibility of miniaturizing the systems for better portability and field-testing.

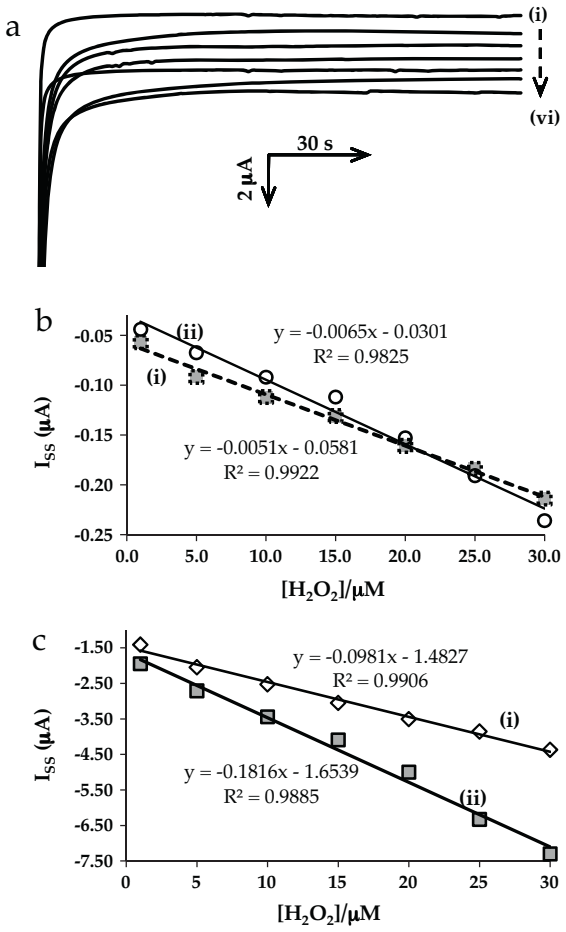

Fig. 8. (a) Amperometric response of SPAuE–PA-SWCNT–MnTAPc at E_{app} = −0.38 V for varied H_2O_2 concentrations: (i) 1.0 μmol L^{-1}, (ii) 5.0 μmol L^{-1}, (iii) 10.0 μmol L^{-1}, (iii) 15 μmol L^{-1}, (iv) 20.0 μmol L^{-1}, (v) 25 μmol L^{-1} and (vi) 30 μmol L^{-1}. Calibration curves, I_{SS} (μA) versus [H_2O_2] (μmol L^{-1}) for (b) SPAuE–PA–MTAPc and (c) SPAuE–PA-SWCNT–MTAPc. M = Co (i) and Mn (ii).

4. Conclusions

The covalent immobilization of PA-SWCNT, CoTAPc and MnTAPc as hybrids for H_2O_2 detection has been accomplished. Several characterization techniques, such as HRSEM, Raman spectroscopy and electrochemistry were used to confirm the presence of the materials immobilized as proposed. The electron transfer rate constants (k_{app}) in $[Fe(CN)_6]^{3-/4-}$ for the PA-SWCNT–MTAPc modified electrodes were higher than other electrodes and this also translated to better electrocatalytic currents for H_2O_2 detection. The use of the screen-printed electrode was important in demonstrating the possible miniaturization of these electrochemical systems for the detection of H_2O_2. The use of these electrodes is continuing for the detection of glucose using immobilized glucose oxidase enzyme. The PA-SWCNT–MTAPc scaffolding will be used as electron mediators, thus forming a second generation of biosensors.

Acknowledgements

This work was supported by DST/Mintek Nanotechnology Innovation Centre (NIC) and by National Research Foundation (NRF) through DST/NRF South Africa Research Chairs Initiative for Professor of Medicinal Chemistry and Nanotechnology as well as Rhodes University.

Appendix A. Supplementary data

Supplementary data associated with this article can be found, in the online version, at doi:10.1016/j.talanta.2011.07.069.

References

[1] G.G. Guildibault, Enzymatic Methods of Analyst, Pergamon, Oxford, 1970.
[2] M.A.T. Gilmartin, R.J. Ewen, J.P. Hart, J. Electroanal. Chem. 401 (1996) 127–137.
[3] P. Mashazi, T. Nyokong, Microchim. Acta 171 (2010) 321–332.
[4] P. Mashazi, C. Togo, J. Limson, T. Nyokong, J. Porphyrins Phthalocyanines 14 (2010) 252–263.
[5] S. Iijima, C. Brabec, A. Maiti, J. Bernholc, J. Chem. Phys. 104 (1996) 2089–2092.
[6] T. Mugadza, T. Nyokong, J. Colloid Interface Sci. 354 (2011) 437–447.
[7] J.H. Zagal, S. Griveau, K.I. Ozoemena, T. Nyokong, F. Bedioui, J. Nanosci. Nanotechnol. 9 (2009) 2201–2214.
[8] D. Nkosi, K.I. Ozoemena, Electrochim. Acta 53 (2009) 2782–2793.
[9] M.D. Ellison, P.J. Gasda, J. Phys. Chem. C 112 (2008) 738–740.
[10] B.N. Achar, K.S. Lokesh, J. Organomet. Chem. 689 (2004) 3357–3361.
[11] J. Obirai, T. Nyokong, Electrochim. Acta 49 (2004) 1417–1428.
[12] J. Pillay, K. Ozoemena, Electrochim. Acta 54 (2009) 5053–5059.
[13] S.-N. Song, D.-M. Li, C.-F. Zhuang, H. Ding, W.-B. Song, L.-F. Ciu, G.-Z. Cao, G.-F. Liu, Eur. J. Inorg. Chem. 184 (2007) 4–1846.
[14] H.L. Anderson, Chem. Commun. 232 (1999) 3–2330.
[15] T. Mugadza, T. Nyokong, Synth. Met. 160 (2010) 2089–2098.
[16] H. Kataura, Y. Kumazawa, Y. Maniwa, I. Umezu, S. Suzuki, Y. Ohtsuka, Y. Achiba, Synth. Met. 103 (1999) 2555–2558.
[17] M.S. Dresselhaus, G. Dresselhaus, A. Jorio, A.G.S. Saito, Carbon 40 (2002) 2043–2061.
[18] R. Saito, T. Takeya, T. Kimura, G. Dresselhaus, M.S. Dresselhaus, Phys. Rev. B 57 (1998) 4145–4153.
[19] E. Smith, G. Dent, Modern Raman Spectroscopy: A Practical Approach, John Wiley and Sons Ltd., Chichester, England, 2005.
[20] P.N. Mashazi, P. Westbroek, K.I. Ozoemena, T. Nyokong, Electrochim. Acta 53 (2007) 1858–1869.
[21] J. Pillay, K.I. Ozoemena, Electrochem. Commun. 9 (2007) 1816–1823.
[22] E. Sabatani, I. Rubinstein, J. Phys. Chem. 91 (1987) 6663–6669.
[23] Z. Li, M. Lieberman, M. Hill, Langmuir 17 (2001) 4887–4895.
[24] P. Mashazi, K. Ozoemena, T. Nyokong, Electrochim. Acta 52 (2006) 177–186.
[25] P. Mashazi, E. Antunes, T. Nyokong, J. Porphyrins Phthalocyanines 14 (2010) 932–947.
[26] E. Ferapontova, L. Gorton, Bioelectrochemistry 55 (2002) 83–87.
[27] E. Ferapontova, V.G. Grigorenko, A.M. Egorou, T. Börchers, T. Ruzgas, L. Gorton, Biosens. Bioelectron. 16 (2001) 147–157.
[28] E. Ferapontova, K. Schmengler, T. Börchers, T. Ruzgas, L. Gorton, Biosens. Bioelectron. 17 (2002) 953–963.